Hindawi
Shock and Vibration
Volume 2019, Article ID 3417598, 8 pages
https://doi.org/10.1155/2019/3417598

Research Article

Study of the Influence of Train Vibration Loading on Adjacent Damaged Tunnel

Yiding Zhao,[1] **Yao Shi**,[2] **and Junsheng Yang**[1]

[1]*School of Civil Engineering, Central South University, Changsha 410075, China*
[2]*CCCC Wuhan Harbour Engineering Design and Research Co., Ltd., Wuhan 430000, China*

Correspondence should be addressed to Yiding Zhao; zhaoyiding89@126.com

Received 16 December 2018; Revised 23 February 2019; Accepted 20 March 2019; Published 2 April 2019

Academic Editor: Fabio Minghini

In this study, the effect of the high-speed train vibration loading on an adjacent damaged tunnel is investigated. Three sets are established to study the effects of the different vibration loadings on the tunnel lining considering the vertical excitation force of the CRH (China Railway High-speed) train. An expression of excitation force for the train vibration loading is applied to simulate the interaction force between wheel and rail, which is set with high-, medium-, and low-frequency responses, and reflects the influences of driving comfort, additional dynamic load, and rail corrugations. The eigenvalue analysis and spring damping absorbing boundary are applied in the numerical simulation. In addition, a quantitative criterion is selected as the allowable vibration peak velocity for the cracked structure. The analysis of the vibration velocity, dynamic deformation, and acceleration of the cracking region show that the secondary lining of this damaged tunnel in set 1 basically has a higher vibration response than that in set 2 for the closer running track. The most adverse working condition with the greatest impact on the lining structure is that two CRH trains simultaneously passing through the cross section in set 3.

1. Introduction

A tunnel is an essential and special underground structure in railway transportation. For the reason that lining structure suffers influences from tunnel site conditions and construction factors, damaging behaviors are commonly observed from construction period to operation period. To ensure the structural stability and safety, more and more attention was paid to the damaging behaviors in the tunnel [1, 2]. Moreover, previously published literature demonstrates that crack is the most common outcome of the damaged tunnel lining structure [3–5].

Dynamic effects may not only cause cracks but also accelerate further development of the existing cracks. So the dynamic response of the tunnel structure cannot be ignored in the realistic engineering project [6–9], which may be caused by the surrounding vibration source [10, 11]. For this reason, the relationship between tunnel and vibration loading must be figured out [12, 13] to ensure safety and stability of tunnel. Nevertheless, few studies have focused on the stability of the damaged tunnel influenced by the train vibration in the adjacent tunnel.

In this paper, a novelty study of a longitudinal crack in a railway tunnel is presented, which focuses on the influence of the train dynamic load on the adjacent structure. The result in this paper can provide valuable guidance for the subsequent reinforcement work and the similar engineering projects located in this area.

2. Engineering Background

2.1. Location and Environmental Condition. The subject railway tunnel in this study is in Zunyi city of Guizhou Province, China (Figure 1), and has 1627 m longitudinal length and 107 m maximum burial depth. The principal stratum, where the railway tunnel is located, is a tilted stratum composed of limestone and mudstone intercalated with limestone. Small amounts of shale intercalated with limestone and coal seam are found near the tunnel. The geology database shows that the surrounding rock is

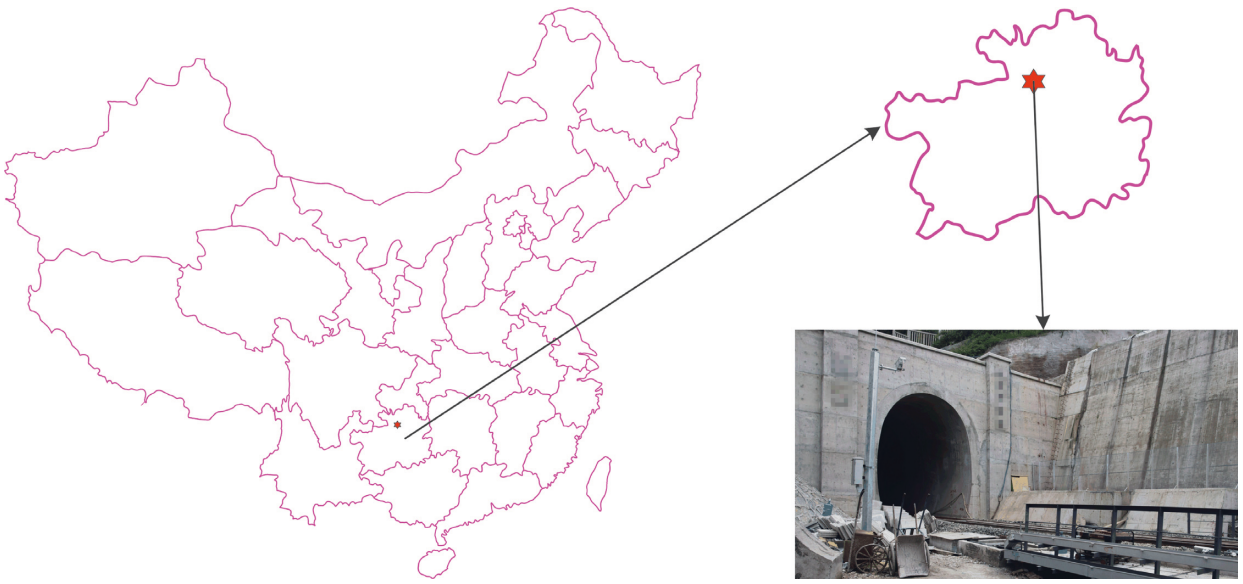

Figure 1: Location of the tunnel.

developed with joint fissures, and the major classification of the underground water is bedrock fissure water. Moreover, there is no obvious seismicity or faultage around the tunnel site. Since the tunnel is located in mountainous topography, the complex topographical conditions cause typical asymmetrical loading on the tunnel trunk in several places. An adjacent high-speed railway tunnel is located at the right side of the railway tunnel, which is in the operation stage.

2.2. Supporting Type of Tunnel. Figure 2 shows the typical cross section of the tunnel, which has 8 m height and 5.5 m width, and is designed as a composite lining structure. In the primary lining, a grid steel frame is arranged with a longitudinal spacing of 1.2 m, a round bar with a diameter of 6 mm is adopted as a steel mesh by spacing of 0.25 m × 0.25 m in the longitudinal and circumferential directions, and C25 [14] shotcrete is used with a thickness of 0.15 m. The grouted anchor rods, whose diameters and lengths are 25 mm and 3 m, respectively, are fixed by the spacing of 1.2 m × 1.2 m in the surrounding rocks after excavation. In the secondary lining, C30 plain concrete with 0.30 m thickness is used. The space between the inverted arch and the pavement is backfilled using C20 rubble concrete.

2.3. Lining Cracking of the Tunnel. After the construction of the tunnel completed, cracks of the secondary lining were observed in this tunnel. The topographic condition, geological condition, and adjacent high-speed railway tunnel were confirmed as the inducements of lining cracking. To visually demonstrate the distribution of the cracks, a panoramic image of the tunnel structure is built as shown in Figure 3. A longitudinal crack initiated at the right sidewall region, such as the blue line in Figure 3. This crack linearly and continuously spreads along the longitudinal direction of the secondary linings and is distributed approximately

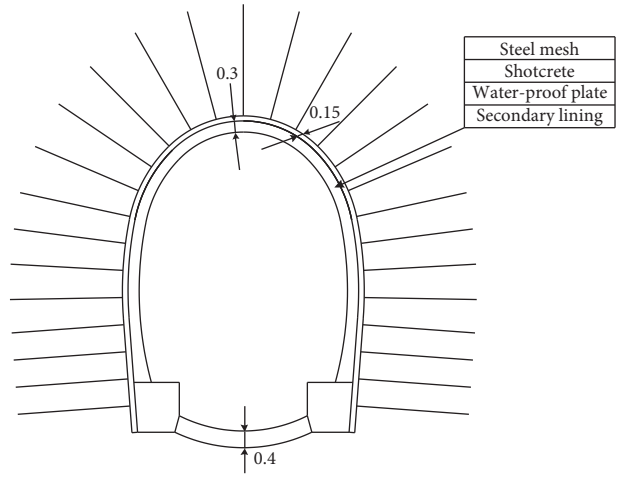

Figure 2: Typical supporting type of the tunnel (unit: m).

within the right sidewall region; the maximum crack width is approximately 4 mm, and the crack depth is greater than 0.2 m.

Because the aforementioned adjacent high-speed railway tunnel is in the operation stage, the effect of the train dynamic load on the cracked lining receives great attention. Figure 4 shows that the space between these two tunnels is very close, from which the altitude difference of the rail surfaces is 2.7 m and the spacing between the tunnel central lines is 14.8 m around the area (40 m in the axial direction) as shown in Figure 3.

3. Methodology

3.1. Simulation of Train Vibration Loading. In this study, the effect of the high-speed train on this cracked tunnel must be investigated, which can provide a reasonable basis for the maintenance schedule. The most important step of the study is to confirm the simulation method of the train vibration

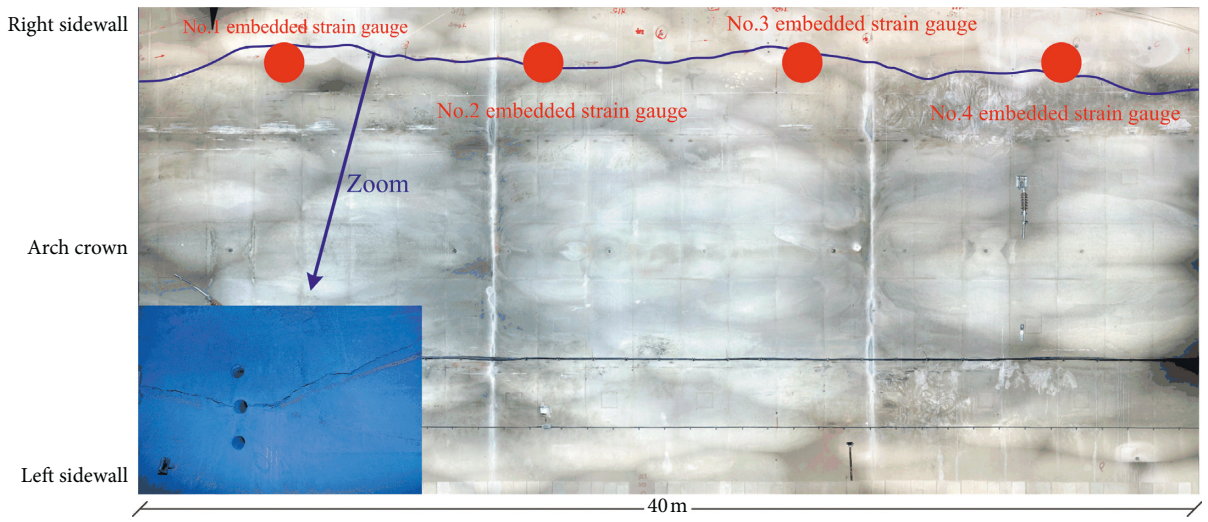

Figure 3: Lining cracking in field.

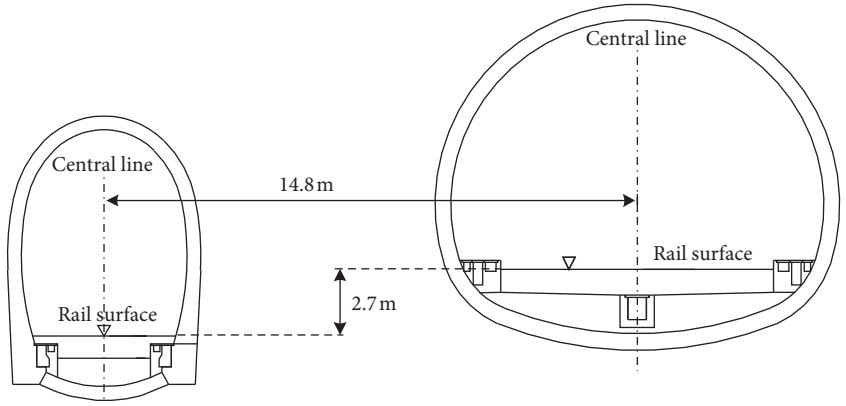

Figure 4: Spacing between two tunnels.

loading. Many theoretical and experimental studies of the British railway technology centre show that the wheel/rail vertical force is always caused by many types of irregularities [11, 15]. The experiments also show that the wheel/rail vertical force mainly appeared in three frequency ranges: (1) low-frequency range (0.5~10 Hz), (2) medium-frequency range (30~60 Hz), and (3) high-frequency range (100~400 Hz). The measured results show that the wheel/rail force is more intense in the middle- and low-frequency ranges, and the high-frequency range mainly affects the vibration response of the vehicle body. For the British track with a train speed of 200 km/h, the management standard of geometric irregularity is shown in Table 1.

An excitation source can be used to simulate the train vibration, which includes the static load and a series of the sine function of the vibration loading. The excitation force for the train vibration loading is used to simulate the interaction force between the wheel and the rail, which is set with high-, medium-, and low-frequency response and can reflect the influences of geometric irregularities:

$$F(t) = P_0 + P_1 \sin w_1 t + P_2 \sin w_2 t + P_3 \sin w_3 t, \quad (1)$$

Table 1: Management standard of geometric irregularity (UK).

Control requirement	Wavelength (m)	Versine (mm)
Driving comfort (I)	50	16
	20	9
	10	5
Additional dynamic load (II)	5	2.5
	2	0.6
	1	0.3
Rail corrugations (III)	0.5	0.1
	0.05	0.005

where P_0 is the static load of the wheel and P_1, P_2, and P_3 are the vibration loads of different control requirements. For the unsprung mass M_0 of the train, the corresponding amplitude of vibration loading is

$$P_i = M_0 a_i w_i^2, \quad (2)$$

where a_i is the versine in three control requirements in Table 1 and w_i is the circular frequency at the wavelength of track irregularity under the corresponding speed. The calculation formula of the circular frequency is

$$w_i = 2\pi \frac{v}{L_i}, \tag{3}$$

where v is the speed of the train and L_i is the typical wavelength that corresponds to the control requirements.

The axle load required by the railway is generally 16~17 t, and the single-side static wheel weight is $P_0 = 80$ kN. The unsprung mass is taken as $M_0 = 750$ kg, and the design speed in the standard is $v = 350$ km/h for a high-speed train. Corresponding to the three control requirements, the typical vibration wavelength and the corresponding versine are taken as $L_1 = 10$ m and $a_1 = 3.5$ mm, $L_2 = 2$ m and $a_2 = 0.4$ mm, and $L_3 = 0.5$ m and $a_3 = 0.08$ mm, respectively. For the CRH (China Railway High-speed) train speed of $v = 180$~324 km/h, the ranges of low frequency, medium frequency, and high frequency are 5~9 Hz, 25~45 Hz, and 100~200 Hz, respectively. In accordance with the above experimental rules, the excitation force is an irregular wave type. For this study, the CRH train speed is $v = 320$ km/h, and the excitation force within 0~2.5 s is shown in Figure 5.

3.2. Boundary Conditions. The reflection of waves in truncated boundary will occur under the fixed boundary condition that results in energy accumulation, which causes a large displacement change of concrete lining. To avoid this influence, the damping boundary is used in the numerical model, which can ensure that the wave energy will spread in the border.

The spring stiffness for the spring damping absorbing boundary is set up by using the coefficient of the subgrade reaction force, and the damping constant per unit area is selected according to the following formula:

$$\begin{aligned} c_{\mathrm{pi}} &= \rho_i \cdot A \sqrt{\frac{\lambda + 2G}{\rho_i}}, \\ c_{\mathrm{si}} &= \rho_i \cdot A \sqrt{\frac{2G}{\rho_i}}, \end{aligned} \tag{4}$$

where c_{pi} is the damping constant per unit area for P-wave, c_{si} is the damping constant per unit area for S-wave, $\lambda = vE/((1+v)(1-2v))$, $G = vE/2(1+v)$, E is the elasticity modulus, v is Poisson's ratio, and A is the area.

3.3. Sets of Numerical Simulation. Three different sets are simulated in this study, as shown in Figure 6, considering the conditions of a single train passing through the left track, a single train passing through the right track, and both trains simultaneously passing through the tracks. There is an observation point to study the influence of the train vibration loading on the realistic cracking location, which is shown as the red dot in Figure 6.

3.4. Establishment of Numerical Model. The numerical model is established for the typical tunnel cross section by the finite element method (FEM), and the mapping mesh of the numerical simulation is shown in Figure 7. The surrounding rocks in the numerical model are simulated by solid elements under the 2D plane strain assumption. Moreover, secondary lining is considered as the ideal elastic material by using the beam element. For the dynamic analysis, an eigenvalue analysis is used to analyse the inherent vibration characteristics of the rock and structure. Through the eigenvalue analysis, the vibration participation coefficient of its natural mode (mode state), natural period (natural frequency), and other characteristics are determined by the mass and stiffness of the structure. These characteristics depend on the mass and stiffness of the structure. Periods of 0.65 s and 0.53 s are selected in this numerical model.

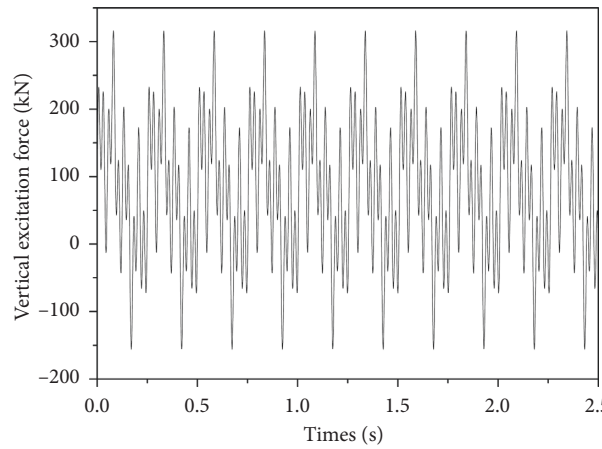

Figure 5: Oscillogram of the simulated vertical excitation force.

The physical properties in the numerical simulation are listed in Table 2, which are obtained from geologic examination and design document. Moreover, the left cracked lining is assumed unbroken in the numerical model, and we only focus on the effect of the vibration loading on the concrete structure.

4. Results and Discussion

4.1. Analysis of the Vibration Velocity. The outputs of the time history curve of the vibration velocity at the observation point are shown in Figure 8. The responding vibration velocity of the lining obviously increases when the CRH train passes through the adjacent tunnel in each set. In set 1, the peak velocity decreases by approximately 5% in the horizontal direction and increases by approximately 20% in the vertical direction compared with that in set 2. The results show that the CRH train passing through the left track has a greater effect on the cracked lining than the right one in full speed. The peak velocity of set 1 in the horizontal direction increases by approximately 90% and that in the vertical direction increases by approximately 31% compared with that in set 3. To establish a quantitative criterion, 2.5 mm/s is selected as the allowable vibration peak velocity for the cracked concrete structure [16]. Thus, the vibration speed peak at the observation point does not satisfy the standard requirements within a certain time range. It can be obtained

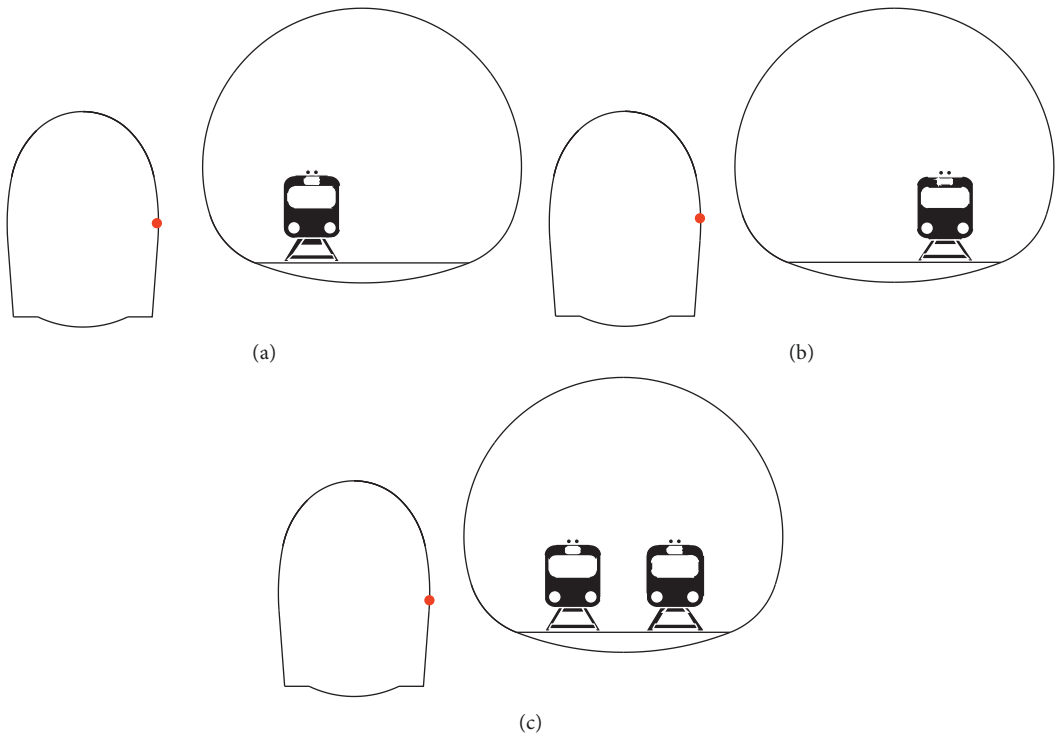

Figure 6: Sets of numerical simulation: (a) 1, (b) 2, and (c) 3.

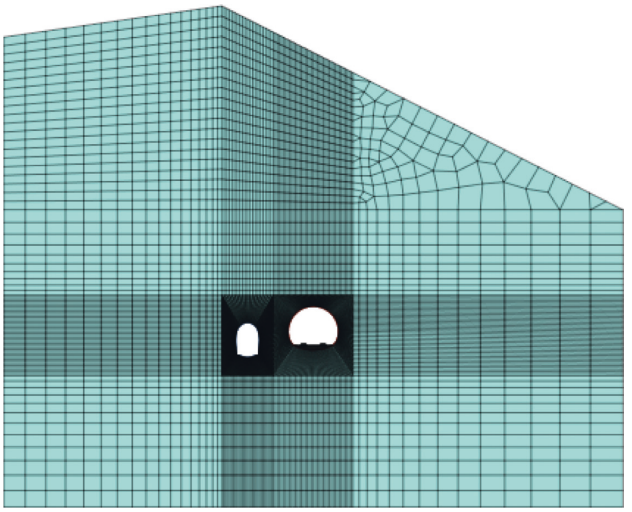

Figure 7: Mapping mesh of the numerical model.

Table 2: Physical properties of the numerical model.

Material	Physical and mechanical parameters
Surrounding rock	$E = 1$ GPa, $\rho = 2200$ kg/m^3, $\mu = 0.32$, $\sigma_s = 150$ kPa, $\varphi = 30^\circ$
Lining of left tunnel	$E = 30.0$ GPa, $\rho = 2500$ kg/m^3, $f_c' = 14.3$ MPa, $f_t = 1.43$ MPa, $\mu = 0.23$
Lining of right tunnel	$E = 31.5$ GPa, $\rho = 2500$ kg/m^3, $f_c' = 16.7$ MPa, $f_t = 1.57$ MPa, $\mu = 0.23$
Filled layer	$E = 28.0$ GPa, $\rho = 2500$ kg/m^3, $f_c' = 11.9$ MPa, $f_t = 1.27$ MPa, $\mu = 0.23$
Steel rail	$E = 210$ GPa, $\rho = 7800$ kg/m^3, $\mu = 0.31$,

that when two CRH trains simultaneously pass through the adjacent tunnel at full speed, the damaged lining should have the maximum vibration velocity. Compared to the 2.5 mm/s allowable vibration peak velocity, the vibration velocity of the observation point in set 1 and set 3 cannot satisfy the requirement.

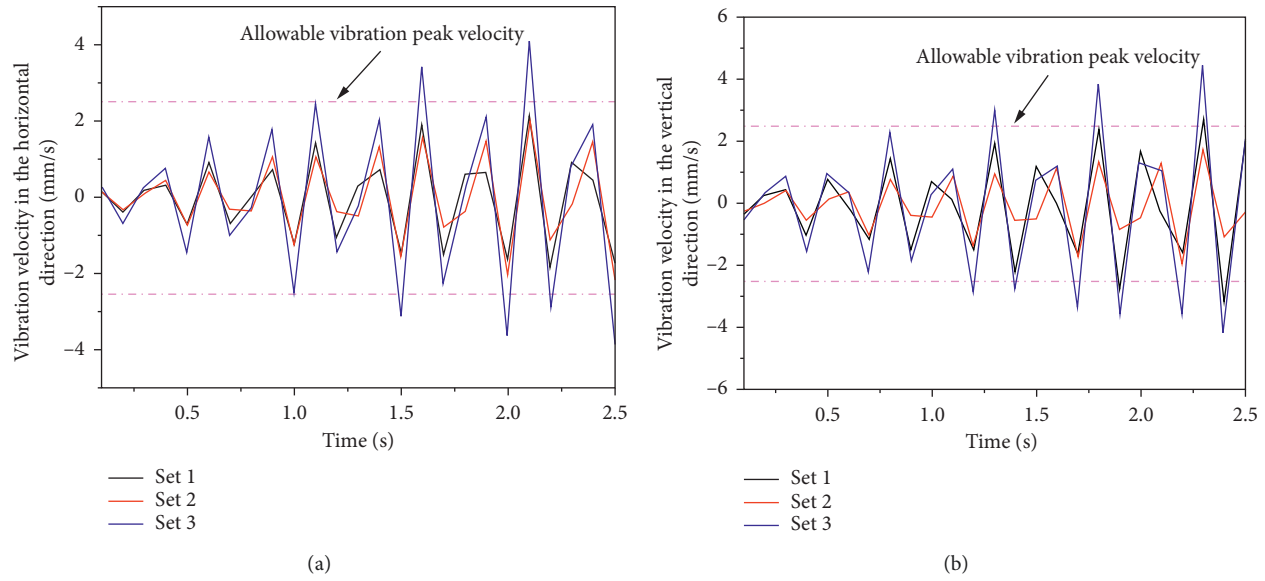

Figure 8: Time history of the vibration velocity of observation point: (a) horizontal direction and (b) vertical direction.

4.2. Analysis of the Dynamic Deformation. In Figure 9, the dynamic deformation of the observation point shows an oscillatory-increasing tendency. The unique variation tendency is caused by the train excitation force in Figure 5, and the maximum dynamic deformation of these three sets is 0.28 mm in set 3. When the excitation force reaches 1.6 s with the maximum excitation force, the dynamic deformation is only 0.04 mm and reaches the peak value of 0.08 mm after 0.2 s in set 1. The curve indicates that there is a peak in each increasing stage and decreasing stage, but the frequency is behind the frequency of the excitation force. The reason for this phenomenon is that the tracks are directly subjected to the dynamic force, which is subsequently transmitted to the concrete filling layer, right lining structure, surrounding rock, and left lining structure. In the process of downward transmission, there is a certain time difference due to the influence of fluctuation through different media and transmission distance. The maximum dynamic deformations of three sets are above 0.1 mm, which implies that the train dynamic load may cause further crack development because the crack is usually in units of millimeter.

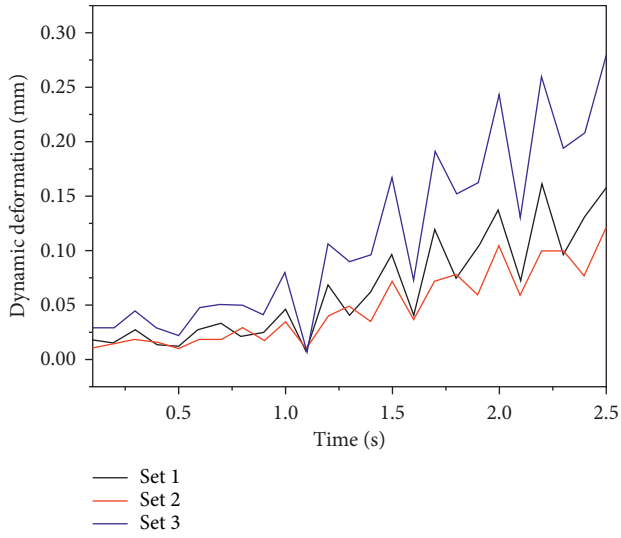

Figure 9: Time history of dynamic deformation of the observation point.

4.3. Analysis of the Dynamic Acceleration. The vibration acceleration oscillates up and down around the zero position, as shown in Figure 10, and the positive acceleration is significantly greater than the negative acceleration. The vibration acceleration does not reach the zero for these three sets when the excitation force reaches zero at 0.29 s for the same reason with the dynamic deformation. Moreover, this result indicates that the response of the dynamic deformation in accordance with the response of the vibration acceleration by comparing Figures 9 and 10, which is affected by the train excitation force. In the related standard, a vibration acceleration of 220 mm/s^2 is the allowable value for avoiding cracking for concrete structure, and 220 mm/s^2 is selected as the criterion in this study for avoiding further development of cracks in concrete structure. Comparing to the numerical results, the maximum vibration acceleration 297.85 mm/s^2 of set 3 in the vertical direction cannot meet the requirement.

4.4. Maintenance Work and Strengthening Effect. Since the train vibration loading, which is verified by numerical results, may cause further crack development, maintenance work [17, 18] must be implemented to ensure the safety of the damaged tunnel. Considering the cracking region and aforementioned inducements of cracks, the detailed maintenance scheme can be summarized as (1) demolishing the 150 mm thick secondary lining from the hance to the ditch cover, (2) reconstructing the secondary lining using

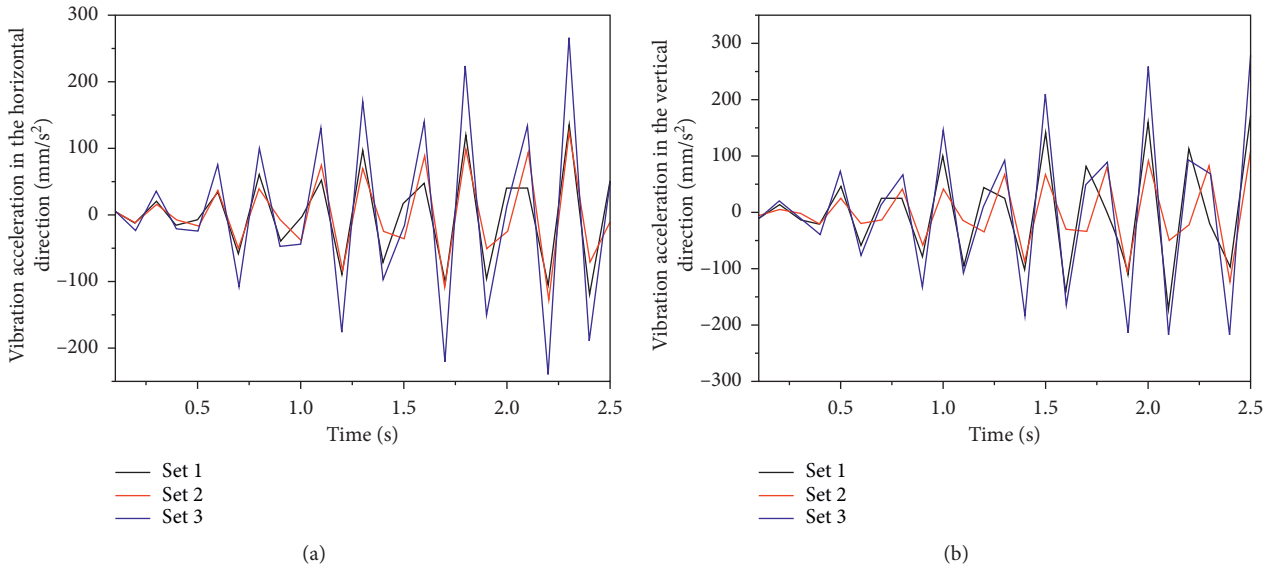

Figure 10: Time history of the acceleration of the observation point: (a) horizontal direction and (b) vertical direction.

Table 3: Outputs of the field test.

M^1 (days)	Cross section of monitoring							
	No. 1		No. 2		No. 3		No. 4	
	S^2 ($\mu\varepsilon$)	T^3 (°C)	S ($\mu\varepsilon$)	T (°C)	S ($\mu\varepsilon$)	T (°C)	S ($\mu\varepsilon$)	T (°C)
0	3349	12.8	33503	12.8	3329	12.6	3323	13.2
13	3296	13.4	3299	14.6	3297	14.4	3283	14.4
28	3305	14.4	3303	14.2	3308	13.8	3305	15.1
41	3302	14.2	3273	14.3	3304	13.9	3310	15.3
72	3294	16.3	3249	16.3	3294	15.7	3301	16.8

[1]Monitoring time; [2]Strain; [3]Temperature.

reinforced concrete with single-layer reinforcing mesh and backfilling to the original designed surface, (3) using embedded steel bars in the new lining to maintain a connection with surrounding concrete, and (4) setting mortar bolt with 1 m spacing in the axial direction for grouting to improve the rock mass condition. To monitor the stability of the rebuilt structure, a test has been applied in field. The strain of the secondary lining [19] is obtained via an embedded strain gauge, which has a measurement range of ±1500 $\mu\varepsilon$ with 0.5% precision and 146 mm gauge length. Four embedded strain gauges (Figure 3) have been installed in different cross sections to monitor the rebuilt lining. Moreover, a comprehensive test instrument is applied for measuring and recording data. The monitoring results of the concrete strain show that the strain value is stable (Table 3), and the maintenance work is effective so far, which implies that the train dynamic load has less impact on the rebuilt lining.

5. Conclusions

This study discusses the effect of the vertical excitation force due to CRH trains on a damaged adjacent tunnel and the effect of the maintenance work. The following points are outlined as the outcomes of this study:

(1) The vibration responding analysis of the surrounding rock-lining-vibration loading model is established by considering the vertical excitation force of the CRH train, which can effectively present the effect of the dynamic load on the damaged tunnel.

(2) The vibration velocity, dynamic deformation, and acceleration of the observation point of this damaged tunnel in set 1 are basically higher than those in set 2 for the closer running track.

(3) In set 3, the vibration velocity of the secondary lining is basically higher than those in set 1 and set 2. The peaks in the horizontal and vertical directions increase by approximately 90% and 31%, respectively, which indicates that set 3 has the most adverse working condition and the greatest effect on the lining structure.

(4) Considering the allowable vibration peak velocity of 2.5 mm/s, the CRH train must reduce speed when running on the left track. Any two CRH trains should avoid meeting in the cracked region, if possible.

(5) It is necessary to implement maintenance work in the damaged tunnel to ensure tunnel stability. Reconstruction and anchoring have been proven as

effective methods to reduce the impact of dynamic load on the damaged tunnel.

Data Availability

The data used to support the findings of this study are included in the article.

Conflicts of Interest

The authors declare that there are no conflicts of interest regarding the publication of this paper.

Acknowledgments

The authors thank the funding provided by the CCCC Wuhan Harbour Engineering Design and Research Co., Ltd. The authors thank Prof. Fabio Minghini's hard work.

References

[1] Y. Jiang, Y. Tanabashi, M. Fujii, X. Zhao, and S. Idenaga, "Database development for road tunnel maintenance and management by using geographical information system (new technology for maintenance/retrofit and renewal works in geotechnical engineering: tunnels, underground structures and antiquities)," *Soil Mechanics and Foundation Engineering*, vol. 52, pp. 25–27, 2004.

[2] F. Sandrone and V. Labiouse, "Identification and analysis of swiss national road tunnels pathologies," *Tunnelling and Underground Space Technology*, vol. 26, no. 2, pp. 374–390, 2011.

[3] Y. C. Chiu, T. T. Wang, and T. H. Huang, "Investigating continual damage of a nineteenth century masonry tunnel," *Proceedings of the ICE—Forensic Engineering*, vol. 167, no. 3, pp. 109–118, 2014.

[4] Y. Zhao, C. Liu, Y. Zhang, J. Yang, and T. Feng, "Damaging behavior investigation of an operational tunnel structure induced by cavities around surrounding rocks," *Engineering Failure Analysis*, vol. 99, pp. 203–209, 2019.

[5] H. W. Huang, D. J. Liu, Y. D. Xue, P. R. Wang, and L. Yin, "Numerical analysis of cracking of tunnel linings based on extended finite element," *Chinese Journal of Geotechnical Engineering*, vol. 35, no. 2, pp. 266–275, 2013, in Chinese.

[6] S. Gupta, H. Van den Berghe, G. Lombaert, and G. Degrande, "Numerical modelling of vibrations from a thalys high speed train in the groene hart tunnel," *Soil Dynamics and Earthquake Engineering*, vol. 30, no. 3, pp. 82–97, 2010.

[7] F. Xue, "Dynamic responses of subway tunnel in clay stratum to moving loads," *Arabian Journal for Science and Engineering*, vol. 42, no. 3, pp. 1327–1340, 2017.

[8] T. Real, C. Zamorano, F. Ribes, and J. I. Real, "Train-induced vibration prediction in tunnels using 2D and 3D fem models in time domain," *Tunnelling and Underground Space Technology*, vol. 49, pp. 376–383, 2015.

[9] Q. Yan, H. Chen, W. Chen, J. Zhang, S. Ma, and X. Huang, "Dynamic characteristic and fatigue accumulative damage of a cross shield tunnel structure under vibration load," *Shock and Vibration*, vol. 2018, Article ID 9525680, 14 pages, 2018.

[10] W. Z. Chen, D. Zhang, and J. X. Yu, "Study on stability of close cross tunnel on existing tunnel," *Chinese Journal of Rock Mechanics and Engineering*, vol. 34, no. 1, pp. 3097–3105, 2015, in Chinese.

[11] J. Lai, K. Wang, J. Qiu, F. Niu, J. Wang, and J. Chen, "Vibration response characteristics of the cross tunnel structure," *Shock and Vibration*, vol. 2016, Article ID 9524206, 16 pages, 2016.

[12] X. Zhang, Y. Jiang, and S. Sugimoto, "Seismic damage assessment of mountain tunnel: a case study on the Tawarayama tunnel due to the 2016 Kumamoto earthquake," *Tunnelling and Underground Space Technology*, vol. 71, pp. 138–148, 2018.

[13] W. L. Wang, T. T. Wang, J. J. Su, C. H. Lin, C. R. Seng, and T. H. Huang, "Assessment of damage in mountain tunnels due to the Taiwan Chi-Chi earthquake," *Tunnelling and Underground Space Technology*, vol. 16, no. 3, pp. 133–150, 2001.

[14] Ministry of Housing and Urban-Rural Construction of the People's Republic of China (MOHURD), *Code for Design of Concrete Structures*, GB 50010-2010, Ministry of Housing and Urban-Rural Construction of the People's Republic of China (MOHURD), Beijing, China, 2015.

[15] H. H. Jenkins, J. E. Stephenson, G. A. Clayton, G. W. Morland, and D. Lyon, "The effect of track and vehicle parameters on wheel/rail vertical vibration loads," *Railway Engineering Journal*, vol. 3, no. 1, pp. 2–16, 1974.

[16] Ministry of Housing and Urban-Rural Construction of the People's Republic of China (MOHURD), *Standard for Available Vibration of Building Engineering, GB 50868-2013*, Ministry of Housing and Urban-Rural Construction of the People's Republic of China (MOHURD), Beijing, China, 2013.

[17] Y. Zhang, C. Liu, W. Lu, H. Xie, and H. Peng, "Comparative study of RC members with strengthening using strain hardening cementitious composite and fiber reinforced mortar," *Journal of Testing and Evaluation*, vol. 47, no. 1, article 20170439, 2019.

[18] Y. Zhang, "Improved numerical approach for evaluating the behavior of reinforced concrete members with flexural strengthening using strain hardening cementitious composite," *Engineering Fracture Mechanics*, vol. 189, pp. 330–338, 2018.

[19] J. Lai, J. Qiu, H. Fan et al., "Fiber bragg grating sensors-based in situ monitoring and safety assessment of loess tunnel," *Journal of Sensors*, vol. 2016, Article ID 8658290, 10 pages, 2016.